Title

Characterization of Repulsive Forces and Surface Deformation in Thin Micellar Films via AFM

Journal

Langmuir, 33(40)

ISSN

0743-7463

Authors

Micklavzina, Benjamin L

Longo, Marjorie L

Publication Date

2017-10-10

DOI

10.1021/acs.langmuir.7b02508

Peer reviewed

Characterization of Repulsive Forces and Surface Deformation in Thin Micellar Films via AFM

Journal:	*Langmuir*
Manuscript ID	la-2017-02508t.R1
Manuscript Type:	Article
Date Submitted by the Author:	n/a
Complete List of Authors:	Micklavzina, Benjamin; University of California Davis, Materials Science and Engineering Longo, Marjorie; University of California Davis, Department of Chemical Engineering

Characterization of Repulsive Forces and Surface Deformation in Thin Micellar Films via AFM

Benjamin L. Micklavzina[†] *and Marjorie L. Longo*[§]

[†]Department of Materials Science and Engineering, University of California Davis, Davis, California, 95616,

[§]Department of Chemical Engineering, University of California Davis, Davis, California, 95616

Abstract

Here we examine how the force on an AFM tip varies as it approaches micellar surfactant films, and use this information to discern the film's surface structure and Young's Modulus. Rows of wormlike hemi-micelles were created at a graphite interface using 10 mM sodium dodecyl sulfate (SDS). We found that the repulsive force on a silicon nitride tip as it approached the surface was exponential, with a decay length of 2.0±0.1 nm. The addition of Na_2SO_4 was found to cause a change in this behavior, with a clear split into two exponential regions at concentrations above 1 mM. We also observed that the range of these forces increased with added salt from ~15 nm in pure SDS to ~20 nm at a Na_2SO_4 concentration of 1.34 mM. These forces were inconsistent with electrostatic repulsion, and were determined to be steric in nature. We show that the behavior at higher salt concentrations is consistent with the theory of

polyelectrolyte brushes in the osmotic regime. From this, we hypothesize the presence of micellar brushes at the surface that behave similarly to adsorbed polymer chains. In addition, the Young's modulus of the film was taken from data near the interface using Sneddon's model, and found to be 80±40 MPa. Similar experiments were performed with 10 mM dodecylamine hydrochloride (DAH) solutions in the presence of added magnesium chloride. The decay length for the pure DAH solution was found to be 2.6±0.3 nm, and the addition of 1.34 mM of $MgCl_2$ caused this to increase to 3.7±0.3 nm. No decay length splitting was observed for DAH. We conclude that the behavior at the surface resembles that of an uncharged polymer brush, as the ionic and surface charge densities are much lower for DAH than for SDS.

Introduction

It has been established in the literature that sodium dodecyl sulfate (SDS) forms wormlike hemi-micelles when exposed to a hydrophobic surface.[1-3] Rows of these micelles form grains that stretch across the surface with grain sizes on the order of 0.1 μm. For highly dynamic surfaces such as lipid and micellar layers, the interface is in constant flux due to thermal fluctuations and local changes in surface density, creating significant steric forces that extend for nanometers away from the surface.[4-5] Studying the distance dependence of such forces could be informative for micellar films, as the strength and structure of the film may correlate to steric forces. Importantly, there may be interesting information about surface structure and the ionic environment hidden in the distance dependence of steric forces.

Moreover, while micellar films may resemble their lipid counterparts, there are good reasons to question whether the surfaces deform similarly. Aside from the obvious difference in surface packing and structure, the micellar surface is much more mobile and fragile. Surfactant

molecules freely desorb and readsorb onto the surface, and the surface is constantly shifting.[2-4] Even moderate disturbance of the surface can cause micellar desorption; for example, direct imaging with an atomic force microscopy (AFM) tip has been known to disperse the micellar film.[6] The study of how surfaces deform when probed with an AFM tip is a thoroughly researched field, and several well established theories exist which can relate the surface deformation to the load force and the Young's modulus of a substrate.[7-10] In the case of thin biological films, it has been shown that these theories can be adapted to determine elastic moduli if information about how the deformation of the film changes with load is known.[9-11] Assuming that the micelles at the surface behave elastically at measurable load forces, it might then be possible to apply adapted versions of these theories to micellar surfaces. Most lipid layer models make use of a stiffness coefficient or Young's modulus, so it should be possible to extract these values for micellar films as long as the film is strong enough to sustain a load while in contact.

Our prior work focused on the study of breakthrough forces for hemi-micellar films using AFM, and characterizing how these forces changed with added salt. We began our experiments by imaging 10 mM SDS and 10mM dodecylamine hydrochloride (DAH) films in soft contact mode via AFM. Shown in Figure 1 is an example AFM image taken of the SDS hemi-micellar film at our graphite interface, as well as a cross-section of the proposed structure.[12] DAH films at concentrations of 10 mM exhibited the same wormlike structure. Our first focus was on how the force required to breach the film (breakthrough force) changed with added salt. Experiments were performed with $MgCl_2$, NaCl, and Na_2SO_4 to determine the effect of the coion and counterion on the surface structure and the breakthrough force. In all cases, it was found that addition of roughly 1.4 mM of salt increased the breakthrough forces observed in the film by 30-70%. The suspected cause of this strengthening was the change in free energy of formation of

these micellar structures. Higher concentrations of salt were not used due to increased turbidity in solution, especially in the case of $MgCl_2$. A detailed study of why this strengthening occurred can be found in our prior work.[12] Consistent observation of breakthrough forces at the surface imply that the film could be robust enough to analyze the data for Young's modulus.[12]

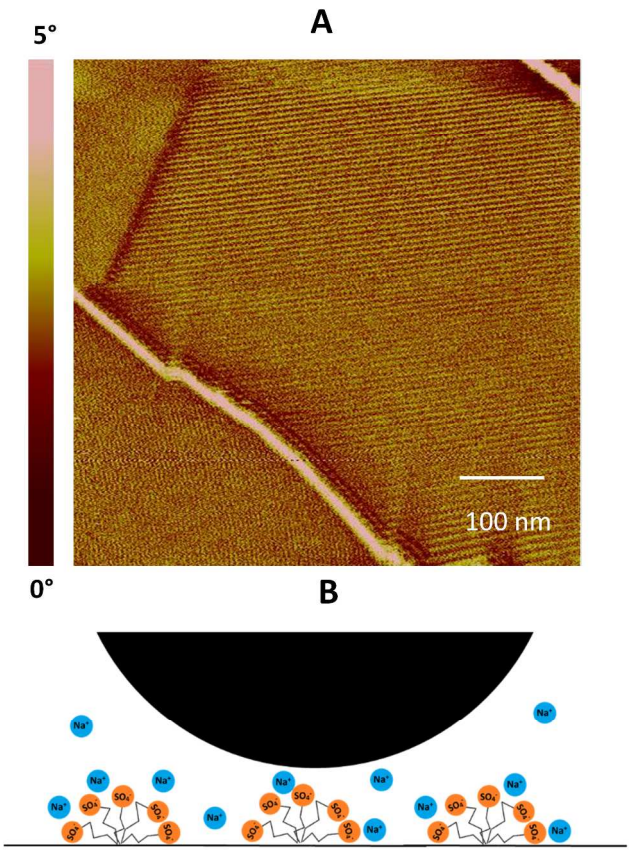

Figure 1. (A) AFM phase image of a 10 mM SDS film in the presence of 2 mM Na_2SO_4 showing rows of hemi-micelles. A grain boundary is present in the top left corner and two graphite steps run diagonally. (B) Cross-section of the proposed structure of rows of hemi-micelles at the surface with a scale-sized tip.

In this work, we examine how the force on the AFM tip changes as it approaches the SDS and DAH hemi-micellar films adsorbed to graphite, and analyze what the cause of longer range

forces may be. Our work will demonstrate the presence of long range forces on the AFM tip which we propose are the result of some previously unreported surface structures, and that these structures can show steric forces similar to charged or neutral polymer brushes depending on the electrolyte environment. In addition, we use previous theory developed for AFM to measure the Young's moduli of SDS films and how they change with added salt concentrations. We will use an estimate to show that the film has a Young's modulus similar to those reported for lipid bilayers.

Materials and Methods

Sodium dodecyl sulfate (SDS) was purchased from Sigma-Aldrich (ACS reagent, ≥99%), and was dissolved in deionized water at a concentration of 10 mM. This 10 mM solution was then placed in contact with ZYH grade highly ordered pyrolytic graphite (HOPG) purchased from MikroMasch. Before each trial, the graphite surface was peeled with clear tape to ensure that the surface was fresh. After contact, the surface was allowed at least 30 minutes to equilibrate with the SDS solution before it was placed into a Dimension 3100 AFM from Veeco for measurement. Measurement was done with MSCT nonconductive silicon nitride tips from Veeco, with nominal spring constants of 0.05 Nm^{-1} and tip radii 2-10 nm. Imaging was done in soft contact mode away from the surface, and all scale data in these images represents either tip deflection or phase data rather than true height as a result. Once the presence of a micellar film at the surface was established by this soft contact imaging, data was taken measuring the force on the tip as it approached the surface. The ramp rate on approach was kept at a constant 50 nms^{-1}. The ramp rate here was kept low to minimize surface disturbances, as higher rates were found to degrade the film over multiple consecutive measurements. Force curves were taken many times ($n \sim 50$) at the same location so as to create a distribution of curves. Significant deterioration of

the film during measurement was not observed so long as the maximum force exerted on the film was not significantly larger than the film's breakthrough force. It was found that changing the region of the graphite being probed caused significant (~10-40%) changes in quantities such as breakthrough forces and decay lengths, so efforts were made to minimize lateral movement of the AFM tip between trials. Qualitative trends remained consistent across films using this methodology.

Sodium sulfate (Na_2SO_4) was purchased from Sigma-Aldrich (ACS reagent, ≥99%), and used to make a 100 mM stock solution in deionized water. Once force curves were measured for the pure SDS film, the tip was moved several micrometers away from the surface and the Na_2SO_4 solution was added in situ to the container holding the SDS. Samples were given between 30-60 minutes to equilibrate before the tip was lowered to the surface to take more measurements. These steps were repeated until the concentration of salt was nearly 1.5 mM or the solution began to display significant turbidity. The procedure described for SDS and Na_2SO_4 was then repeated using dodecylamine hydrochloride (DAH) purchased from TCI America (≥98%) with magnesium chloride hexahydrate ($MgCl_2$) purchased from Sigma-Aldrich (ACS reagent, ≥99%) replacing the salt.

For trials performed starting with bare graphite, the graphite was exposed to deionized water for 30 minutes and then force curves were taken. DI water was then extracted and replaced with our SDS stock solution until the desired SDS concentration was reached. An hour was allowed for equilibration before imaging was done or repulsive forces were measured. Sodium sulfate was added without subtraction of solution for high salt trials, as the small volume of Na_2SO_4 stock solution required meant that the overall SDS concentration would be nearly unchanged by the addition.

For fitting purposes, force curves were transferred to Excel 2013. Empirical forms of relevant equations were fitted using least square residuals for the log force, to provide a weighting for forces at lower overall magnitudes. Residuals were minimized using the solver add-in, and the coefficients of fit were recorded. Thickness of the film in these models was assumed to be 1 nm. In situations where a roughly exponential force curve was observed, an empirical single exponential equation was used to model the decay length in these regions. The thickness of the film at breakthrough was measured manually for each force curve.

Results and Discussion

Force vs Separation Curves. Building on our previous work, we will now study how the force on an AFM tip varies as it approaches an SDS film adsorbed on graphite while changing electrolyte concentration. Shown in Figure 2 is an example of how such data can be analyzed. The repulsive force away from the surface is roughly exponential at most separations. The intersection of the projection of this exponential force into the film with the breakthrough force provides an estimation of the film thickness and the true point of contact between the tip and the hemi-micellar surface. Combining this information with the separation at breakthrough can give an estimation of strain at failure for the micellar films. The exponential force can also be fit to an equation of the form

$$F = Ae^{-\frac{z}{\lambda}} \quad (1)$$

Where F is the force on the tip, z is the tip-sample separation, and A is a fitting constant to give a decay length λ. While results were obtained for an adsorbed film formed in 10 mM SDS with several added salts, we will focus our analysis on the clearest dataset (Na_2SO_4) with the least noise and fewest disturbances to see what conclusions can be drawn.

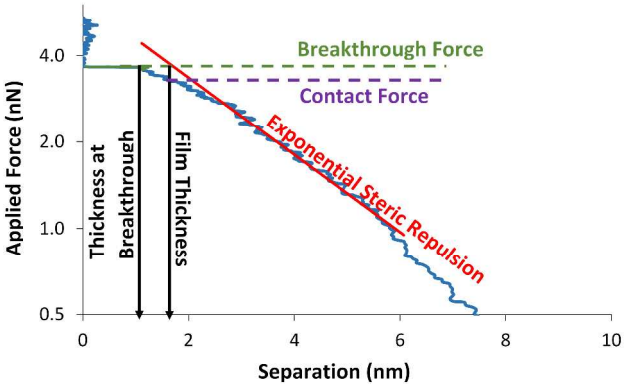

Figure 2. Diagram displaying how each quantity measured was taken from a force vs. separation curve. This curve is from the 10 mM SDS dataset in the absence of added salts.

Our force vs. separation results for an adsorbed hemi-micellar film formed in10 mM SDS with added Na_2SO_4 are shown in Figure 3, and display some interesting qualities. When only SDS is present in solution (no salt), we observe a single decay length (λ_2) for our repulsive forces. As salt concentration increases, the single decay length becomes two distinguishable decay lengths (λ_1, λ_2). The values of these decay lengths as they vary with concentration, as well as the separation at which the transition from λ_1 to λ_2 occurs are shown in Figure 4. The values of the decay lengths show very different trends with increasing ion concentration. The magnitude of λ_2, which is dominant at larger distances from the surface, is a nearly invariant 2.0$\pm$0.1 nm. In contrast, the magnitude of λ_1 increases from 3.0 $\pm$0.2 nm at a Na_2SO_4 concentration of 0.24 mM to 6.9$\pm$ 0.3 nm at 1.34 mM. The presence of split decay lengths was only intermittently present in the absence of added salts. The distance at which this transition occurs also appears to increase with increasing salt concentration, with transitions occurring at 5$\pm$1 nm when salt is not present and 10.9$\pm$0.4 nm at a Na_2SO_4 concentration of 1.34 mM.

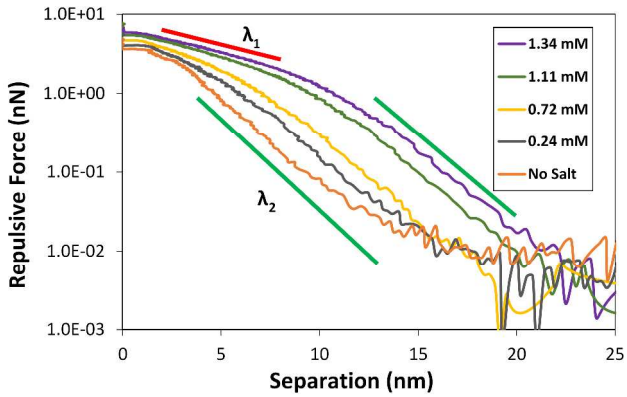

Figure 3. Representative force vs separation curves taken for adsorbed 10 mM SDS in the presence of added Na_2SO_4. The red (λ_1) and green (λ_2) lines represent the regions over which each decay length is dominant.

It is important to understand what mechanism is causing these repulsive forces before continuing analysis. In literature, it is often assumed that the primary force involved in these surface interactions is electrostatic repulsion.[2, 13] However, there are some discrepancies between this interpretation and our data that are not easily resolved. We can estimate what our expected force due to electrostatic repulsion might be between our tip and surface from DLVO theory. The force due to electrostatic repulsion between a spherical tip and a planar surface is given by the relation[4]

$$F_e = \frac{4\pi\sigma_s\sigma_t R\lambda_D}{\varepsilon\varepsilon_0} e^{\frac{-z}{\lambda_D}} \quad (2)$$

where σ_s is the charge density at the surface, σ_t is the charge density of the tip, λ_D is the Debye length, ε is the relative permittivity of water, ε_0 is the permittivity of free space, and z is the distance from the surface. We can calculate the Debye length, assuming we know the concentration of free ions, using the equation[4]

$$\lambda_D = \left(\frac{\varepsilon\varepsilon_0 kT}{e^2 N_A \sum_i^n z_i^2 C_i}\right)^{\frac{1}{2}} \quad (3)$$

where e is the elementary charge, N_A is Avogadro's number, z_i is the charge of ion species i, C_i is the concentration of ion species i, and k is the Boltzmann constant. If we assume that surfactant molecules in the micellar phase are 27% dissociated[14] and that the CMC is 7.8 mM from our previous work,[12] we arrive at a Debye length of 3.3 nm before any Na_2SO_4 is added to our 10 mM SDS solution. This is significantly larger than our observed decay length in the case of pure 10 mM SDS. The addition of 2 mM of Na_2SO_4 would cause a decrease in this length to 2.8 nm, which is still significantly different from our λ_2. Using a tip charge density of -10 mC/m^2 consistent with aged silicon nitride,[15] a σ_s of -60 mC/m^2 for our surface,[12] a tip radius of 6 nm, and a Debye length of 3.3 nm we arrive at a total force at the surface of 0.2 nN after using equation (2). This is much smaller than our observed forces of 3.0 $\pm$ 0.3 nN, even though the tip charge density we are using is conservatively large. Equations (2) and (3) also suggest, when viewed together, that the overall repulsive force should decrease as ions are added to solution. This, however, is opposite of our observed trends, and implies the forces we are observing are not consistent with electrostatic repulsion.

Another issue with assuming electrostatic repulsion is the dominant force in our data comes from our results on decay lengths λ_1 and λ_2. Equation (2) implies that at least one of our observed decay lengths, assuming that it is the result of double layer repulsion, should be equal to the Debye length. If this were the case, we would see a decrease in decay length with increasing concentration of ions. Since we see that is not true for either decay region, we infer that our observed forces in Figure 3 are not the result of electrostatic repulsion.

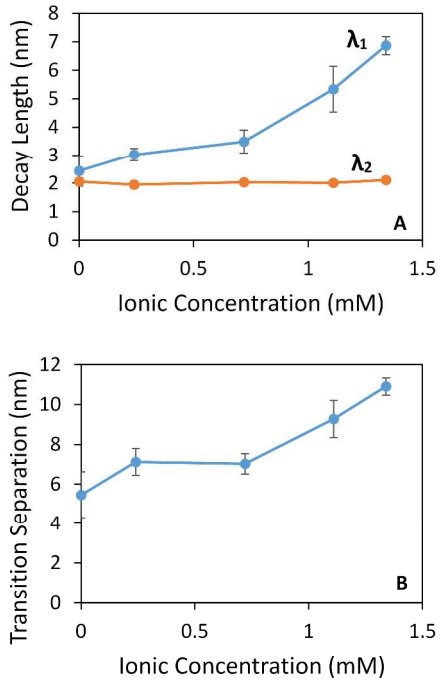

Figure 4. (A) The decay lengths λ_1 and λ_2 from force vs separation curves of adsorbed 10 mM SDS measured as a function of ionic concentration and (B) The AFM tip separation from the graphite surface at which the transition from λ_1 to λ_2 occurs. Ionic concentrations represent the amount of added Na_2SO_4 in solution. Error bars represent the standard deviation of measured decay lengths at each concentration.

If these are not electrostatic forces, there are several alternative explanations to explore. For amphiphilic surfaces, there are four generally recognized forces to investigate: Undulation, peristaltic, protrusion, and steric forces.[4-5] We can quickly rule out the role of undulation and peristaltic forces, as our film is a series of separate wormlike micelles rather than a single contiguous membrane. Even if these forces were present between the film and the tip, they would present a D^{-n} dependence instead of the observed exponential decay shown in Figure 3.[4] This leaves only protrusion and steric forces, both of which follow the general form given in

equation (1). While it is conceivable for protruding molecules to be present at the surface, the expected protrusion decay length for an SDS film can be calculated from known quantities as being on the order of 0.1 nm.[4-5, 16] This is far too small for us to conclude that molecular protrusion is responsible for our observed forces. There is also no mechanism in the theory of protrusion that allows or predicts the emergence of a second decay length or a deviation from strictly exponential behavior.

This leaves only the forces resulting from steric repulsion. Unlike protrusion forces, steric forces are the result of compression of molecules that are constrained between two surfaces. The theory for such forces largely comes from the study of polymers adsorbed at surfaces.[5, 17-18] At lower surface density, the decay length for such steric forces corresponds to a radius of gyration for the polymer molecule.[4, 19] While the individual SDS molecules are too small for our observed values of λ_1 and λ_2 to represent molecular gyration radii, the micellar structures formed by these molecules are known to have radii of gyration between 1.5-2.0 nm.[20-21] Therefore, we speculate that the observed repulsive forces are the result of collective structures, rather than the individual molecules. A drawing of the proposed possible steric structures can be found in Figure 5, showing the different kinds of structures that we might expect to see at the surface. We currently lack the information to distinguish which of these structures is present, as such surface structures have not been imaged directly.

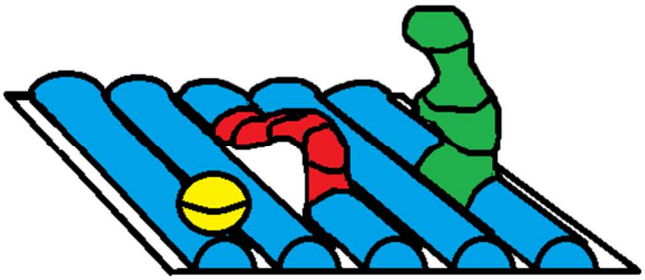

Figure 5. Several possible steric surface structures that might be responsible for long range steric repulsion. From left to right, they are (yellow) adsorbed micelle, (red) two-point wormlike micelles, and (green) single-point wormlike micelles.

Polyelectrolyte Brush Model. Because our surface hemi-micelles have significant surface charge along their length, we will attempt to model our steric surface structures in the same manner as one would model polyelectrolyte brushes, and refer to them, in general, as micellar brushes. For polyelectrolyte brushes, there are two distinct regimes of behavior: the osmotic regime and the salted regime.[22-23] In the osmotic regime, the counterion concentration within the chain's occupied volume is greater than the concentration in the bulk. This creates a net osmotic pressure, and leads to an overall expansion of the film. In the salted regime, the concentration of ions in the bulk exceeds that in the brush, which leads to screening of the charges along the chain and a general contraction of the film. In our previous work,[12] we used modified Grahame equations to determine that the counterion concentration was roughly 1.5 M at the hemi-micellar surface and 8-10 mM in the bulk. This implies that we should be looking at the osmotic regime, as our concentration of ions near the surface should always be greater than in the bulk due to the presence of a diffuse double layer. The force on a polyelectrolyte chain in this regime can be estimated as[22]

$$F = \frac{3LkT}{Na^2} - \frac{\alpha NkT}{L} \quad (4)$$

where L is the length of the chain, k is the Boltzmann constant, T is temperature, a is the Kuhn length, α is the ratio of counterions within the chain volume to charges at the chain surface, and N is the number of Kuhn lengths per chain. Here the first term is an elastic force that resists chain extension, and the second term is an opposing expansion force resulting from counterion osmotic pressure. From this, it can be deduced that the equilibrium chain length obeys the relation[22]

$$L_0 \propto \alpha^{\frac{1}{2}} N a. \quad (5)$$

Where L_0 is the equilibrium chain length at which $F = 0$ from equation (4). For polyelectrolytes, this indicates that the equilibrium chain length in the osmotic regime is independent of surface density of chains, Γ, or external electrolyte concentration. The interaction energy G between surfaces is then[22]

$$G = \int_{L_0}^{z} F(L)dL = \Gamma \alpha N k T \left(A_1 \left(\frac{z^2}{L_0^2} - 1 \right) - A_2 ln \left(\frac{z}{L_0} \right) \right) \quad (6)$$

Using equation (6) and the Derjaguin approximation, which relates the repulsive force to the interaction energy between surfaces, the force of such a polyelectrolyte film on our AFM tip can be estimated by the equation[22]

$$F(z) = 2\pi R \Gamma \alpha N k T \left(A_1 \left(\frac{z^2}{L_0^2} - 1 \right) - A_2 ln \left(\frac{z}{L_0} \right) \right) \quad (7)$$

where Γ is the surface density of chains, R is the radius of the tip, and A_1 and A_2 are arbitrary fitting constants. Fitting to equation (7) is simpler than it might appear, as it is not necessary to know or guess values in the term outside the brackets. These terms can be incorporated into the constants A_1 and A_2, and subsequent fits do not assume specific values for these prefactors. Equation (7) produces reasonable fits for our force curves at higher concentrations of Na_2SO_4.

Examples of fits for our 10 mM SDS film using equation (7) are given in Figure 6A. The values for these fits give ranges of L_0~15-20 nm and $\frac{A_2}{A_1}$~1.5-4 for Na_2SO_4 concentrations at or above 0.72 mM. These values for L_0 are consistent in scale with our observed range of force at these salt concentrations. The ratio $\frac{A_2}{A_1}$ is indicative of the relative strength of osmotic forces to elastic forces in the micellar brushes, and is similar to the value of 2.2 reported by Balastre et al. for PtBS-NaPSS diblock copolymers at low salt concentrations.[22]

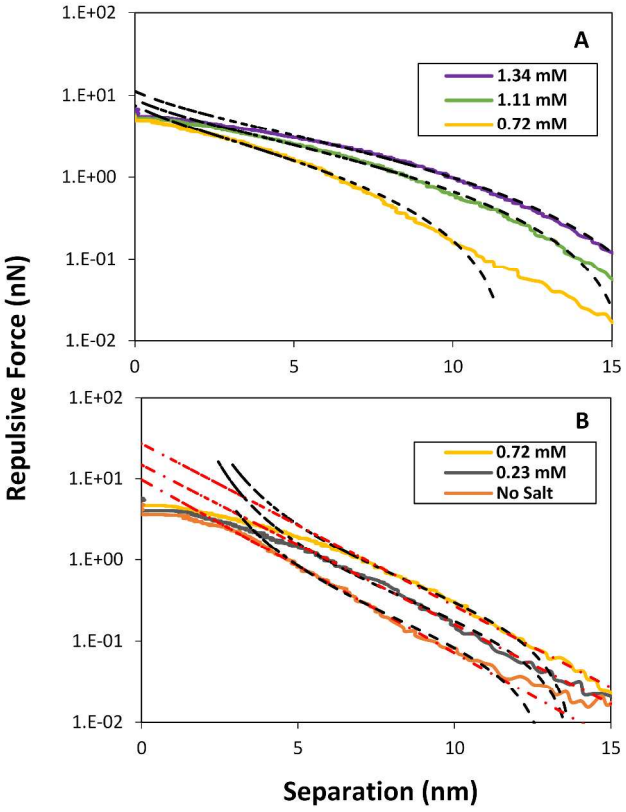

Figure 6. Example force vs separation curves of adsorbed 10 mM SDS at different concentrations of added Na_2SO_4. For (A), black dotted lines represent theoretical fits to equation (7) for each force curve. The values used for the fitted constants here are (1.34 mM) L_0 =19.0 nm, $\frac{A_2}{A_1}$ =2.0, (1.11 mM) L_0 =16.5 nm, $\frac{A_2}{A_1}$ =2.4, (0.72 mM) L_0 =16.2 nm, and $\frac{A_2}{A_1}$ =1.6. For (B),

black dotted lines represent theoretical fits to equation (8) and red dotted lines represent fits to equation (9). The values of L_0 used for the black lines in (B) are (0.72 mM) $L_0 = 12.8$ nm, (0.23 mM) $L_0 = 12.9$ nm, and (No Salt) $L_0 = 12.1$ nm, while the values used for the red lines are (0.72 mM) $L_0 = 13.7$ nm, (0.23 mM) $L_0 = 13.9$ nm, and (No Salt) $L_0 = 12.8$ nm. Fits in (A) were performed using the residuals of points between ~3 nm and ~20 nm, while fits in (B) were done in the range of ~5 nm to ~15 nm.

It is important to discuss, however, why the theory of equation (7) breaks down at low salt concentrations, where the data approaches single exponential behavior in the force curves. Unlike true polymers in the osmotic regime, the value of L_0 in our system is not independent of salt concentration. There is strong evidence for this from our force curves in Figure 3, where the separation at which the film begins to interact with the tip increases as salt is added to solution. In polyelectrolyte brushes this interaction distance is indicative of the uncoiled length of the polymer, Na, and it makes sense that the same would be true here.[22] Unlike polymer brushes, micellar structures can freely change length under differing conditions. The reason for this lengthening is likely linked to the thermodynamics of formation for these structures. While it is possible that there is a kinetic component to this lengthening phenomenon, studies have indicated that the rate of adsorption for SDS onto a hydrophobic surface is nearly constant above the CMC.[24] As salt is added to solution the critical micelle concentration (CMC) drops significantly, indicating that micellar structures are becoming more thermodynamically stable.[12, 25] This increases the likelihood of observing larger micellar structures at the surface and results in a larger observed micellar brush length. It may also indicate that the reason equation (7) fails at

low salt concentrations is that the micellar brush length falls below some critical value beneath which the theory breaks down.

For polyelectrolyte brushes beneath this critical length, most of their surface is in direct exposure to the surrounding fluid. Because of this, the capacity for these structures to swell due to some internal osmotic pressure vanishes, and they behave similarly to an uncharged polymer brush. It has been well established by de Gennes' theory that the pressure between a surface and an uncharged polymer brush can be estimated by the relation[4, 26]

$$P(z) \sim kT\Gamma^{3/2}\left(\left(\frac{z}{L_0}\right)^{-\frac{9}{4}} - \left(\frac{z}{L_0}\right)^{\frac{3}{4}}\right) \qquad \text{For } z < L_0. \tag{8}$$

This relation is roughly exponential in the range $0.2 < \frac{z}{L_0} < 0.9$, and can be estimated in this region by the equation[18, 27-29]

$$P(z) \sim 100kT\Gamma^{3/2}e^{-2\pi z/L_0}. \tag{9}$$

Shown in Figure 6B are curves for low salt concentrations fitted to equations (8) and (9). Fitted values for L_0 for these equations were generally in the range of 12-14 nm, and the decay length was then 1.9-2.2 nm. These values for L_0 are consistent with our assumptions about the critical length, as they are smaller than those observed in the osmotic regime. The quality of fit for equation (9) is clearly better than that of equation (8) in Figure 6B. This is because, while equation (8) is considered accurate for high molecular weight polymers, single exponential equations such as equation (9) have been shown to work best for lower molecular weight systems such as lipid bilayers.[4] Attempts to fit equation (8) and (9) to higher salt concentrations than shown in Figure 6B failed, as neither function could account for the shift from the λ_1 to λ_2 region.

Imaging Surface Structures. While we have offered a theory that could explain our observed repulsive forces, we have not shown any attempt to image the proposed micellar brush structures. Given in Figure 7 are the results of an experiment originally intended to see if such structures could be imaged. We began by looking at the force on the AFM tip at the graphite surface when SDS was absent. This allowed us to establish that the tip was not contaminated with any organic layer, as the results shown in Figure 7A are consistent with a clean tip on bare graphite. SDS stock solution was added in situ, and the tip and surface were give an hour to equilibrate at a concentration of 10 mM before imaging. Images and force curves were recorded for the same surface (Figures 7B, 7D, and 7E), with images taken at differing amounts of force. We sought here to determine if evidence of our hypothesized structures existed at higher imaging forces. The hemi-micellar structures depicted in Figure 1 are clearly present at our surface. However, large protrusions on the order of 10 nm, which our force curves predict are present, are not observed in our images at either low (Figure 7D) or high (Figure 7E) imaging forces. Some adhesion was seen at forces near the breakthrough, though this is not indicative of our proposed structures.

We then added Na_2SO_4 in situ to a very high concentration of 3 mM, and observed how the force curves changed. Our purpose here was twofold: to establish that the decay length splitting in Figure 3 was present for a clean tip, and to lengthen our hypothesized structures so that they might be easier to image. Force curves taken at this high salt concentration show an excellent match (Figure 7C) to predictions from equation (7), but no brush-like structures were apparent regardless of imaging force (data not shown). It's possible that imaging these structures may result in them receding into the surface or dispersing, which could explain why they do not appear in our results. AFM is rarely ever used to image mobile soft structures such as those we

have hypothesized, so the failure to image these features is not entirely unanticipated. Assuming they exist, resolving their presence may require an imaging or detection method that does not disturb the surface yet is extremely high resolution. Techniques such as imaging ellipsometry[30] could be useful tools in the future for confirming the presence of these structures.

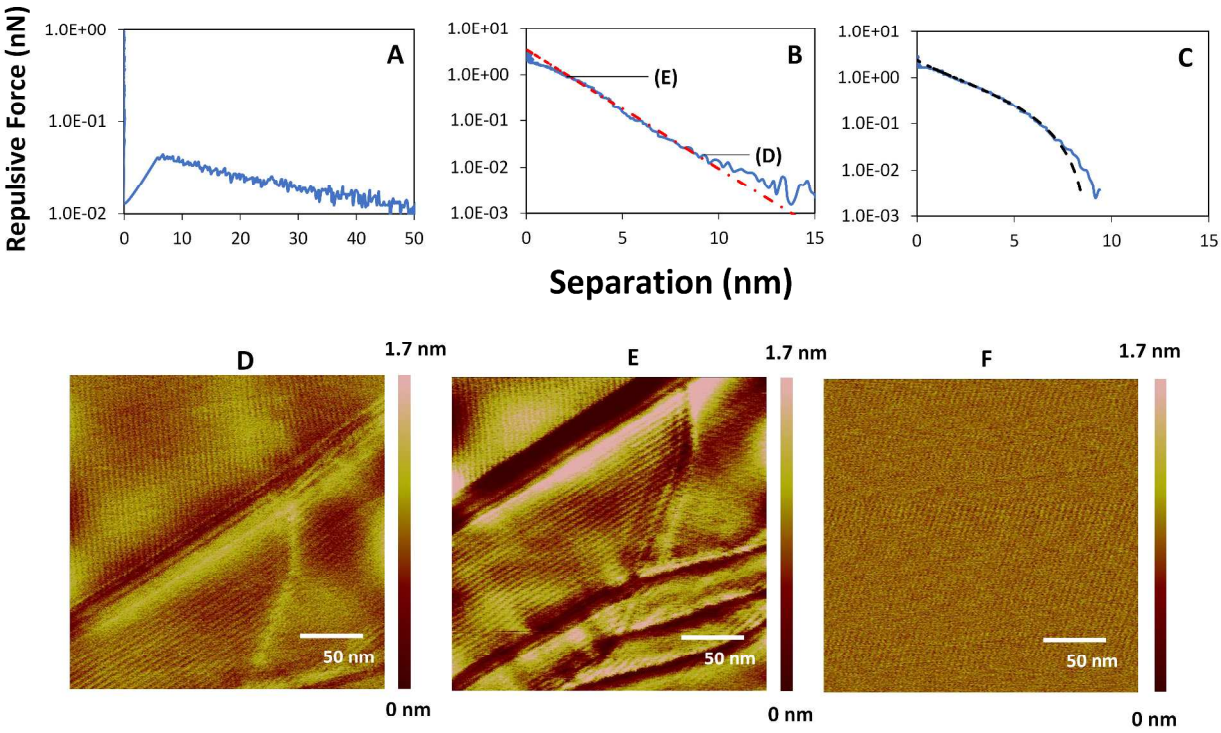

Figure 7. Force curves taken for (A) bare graphite, (B) adsorbed 10 mM SDS, and (C) adsorbed 10 mM SDS with 3 mM Na_2SO_4. The images shown in (D) and (E) were taken in the 10 mM SDS solution, and were taken at roughly the same location. The dotted red line in (B) represents a fit to equation (8) with L_0 =10.62 nm. The indicated points in (B) correspond to the imaging forces for (D) and (E). The black dotted line in (C) represents a fit to equation (6), with fitting constants L_0 =10.23 nm and $\frac{A_2}{A_1}$ =1.9. The image in (F) was taken at the high salt concentration used in (C), and was taken during the same trial as all other images.

Stress and Strain at Failure. One of our early goals was to map how the hemi-micellar film deformed while in contact with our tip, as we believed this could yield information about elastic moduli. Models have been devised for lipid bilayers and monolayers that yield characteristic stiffnesses using data from nanomechanical film deformation with an AFM tip.[7, 10, 31] Unfortunately, the regions of our curves that might yield this information are far too narrow and contain too few data points to realistically use these models. For our SDS data, however, we have been able to extract information about the stress and strain at failure, and from there we can calculate an approximate Young's Modulus.

Making use of this information requires several assumptions. First, we are assuming that the region of contact before the breakthrough instability is a region of elastic deformation. This is justifiable, as similarly structured lipids films are assumed to behave elastically until a yield stress is reached.[11] It is difficult to confirm this assumption in our system, as we have so few data points in contact with our film. In addition, the fact that we breach our film and have surface adhesion implies that confirmation of elastic behavior cannot be obtained from retract curves. Because of this uncertainty, we are assuming that the plastic regime begins at the breakthrough instability, where the film rapidly deforms beneath the tip. Since our sample is thin, we use Sneddon's equation for a perfectly elastic material in the form[7]

$$E = \frac{1}{4\sqrt{Rs}}(1-\nu^2)\frac{dF}{ds} \quad (10)$$

where E is the Young's modulus, R is the radius of the tip, s is the indentation depth, ν is the Poisson's ratio of the film, and $\frac{dF}{ds}$ is the slope of the force vs separation curve in the region of contact. It should be noted that this equation calculates instantaneous Young's modulus, and

assumes that it varies with indentation depth. Since we have so few data points in the direct contact region, we instead estimate the $\frac{dF}{ds}$ term as a single value taken from

$$\frac{dF}{ds} = \frac{F_{breakthrough} - F_{contact}}{s_{breakthrough} - s_{contact}} \quad (11)$$

where the terms are defined in the diagram of Figure 2. Using a nominal tip radius of 6 nm and a Poisson's ratio of 0.5 similar to that of an incompressible lipid layer[32], we calculated the Young's modulus at each Na_2SO_4 concentration. Our results, shown in Figure 8, indicate that the observed Young's modulus is largely unaffected by salt concentration, remaining at about 80 MPa with standard deviation of roughly 40 MPa. When the combined results of each trial modulus are viewed in a histogram, a bimodal Gaussian distribution appears with centers at 65 MPa and 120 MPa. The bimodal distribution may represent the location of the center of the AFM tip relative to the rows of hemi-micelles, i.e. between two rows or on top of one row. It is, however, possible that this is not a true bimodal distribution due to the relatively small number of data points collected. As such, we should be wary of drawing firm conclusions about their meaning here. These values are of the expected magnitude, and are slightly lower than those reported for sturdier lipid films of 100-400 MPa also measured by AFM force measurements of a supported film[9, 31], which is consistent with expectations given our more loosely organized surface structures.

Our estimates, and any such measurement made using a supported film, will generally overshoot the actual film modulus, as the measured Young's modulus for such a thin film is actually a composite of the film's modulus and the substrate's beneath it.[7] This is because the film is constrained between the tip and surface, and the deformation at high loads is limited as a result. Numerous models exist which relate the measured modulus to the true film modulus, but

they generally require more information about how the Young's modulus changes with indentation depth to get accurate data. Since we lack this information due to the narrow region of direct contact, we must restrict ourselves to this estimation.

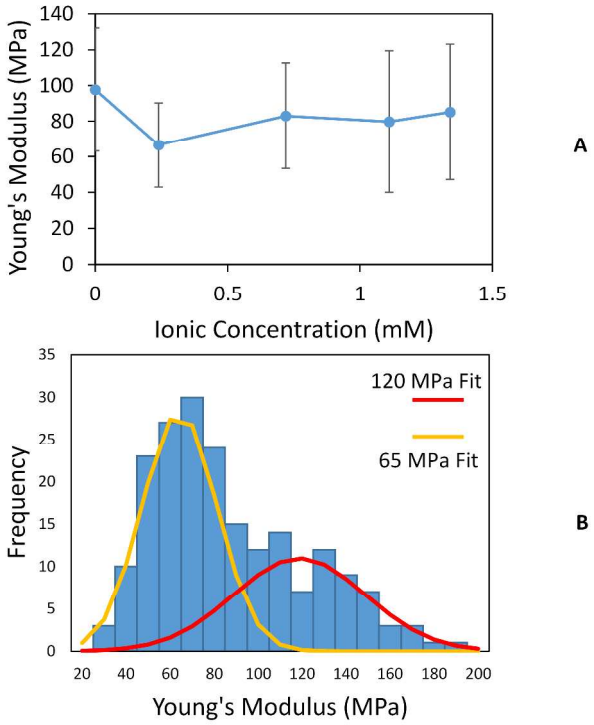

Figure 8. (A) The measured Young's modulus of adsorbed 10 mM SDS as it relates to Na_2SO_4 concentration and (B) the combined histogram of all Young's modulus measurements for SDS with Gaussian fits given. Error bars represent the width of the standard deviation.

DAH Films. Experiments were also performed with a 10 mM DAH film in the presence of added salts. While results were obtained for both NaCl and $MgCl_2$, our analysis will focus on the $MgCl_2$ dataset because it is the less noisy of the two. The resulting force curves at varying concentrations of $MgCl_2$ are shown in Figure 9. We can see that, similar to the case of SDS, increasing the salt concentration generally causes a corresponding increase in the breakthrough forces by 40-60% at added salt concentrations of 1.45 mM. However, there are some interesting

differences in the case of our DAH film which should be addressed. Unlike the case of 10 mM SDS, we see that there is only one characteristic decay length for all salt concentrations. This decay length is not a constant, but changes with salt concentration from 2.6±0.3 nm in its absence to 3.7±0.3 nm when the $MgCl_2$ concentration is 1.45 mM. Multiplying by 2π, these decay lengths imply by equation (9) that the micellar brush layer thickness changes from approximately 16 nm to 24 nm, i.e. above the critical brush length suggested by the SDS results.

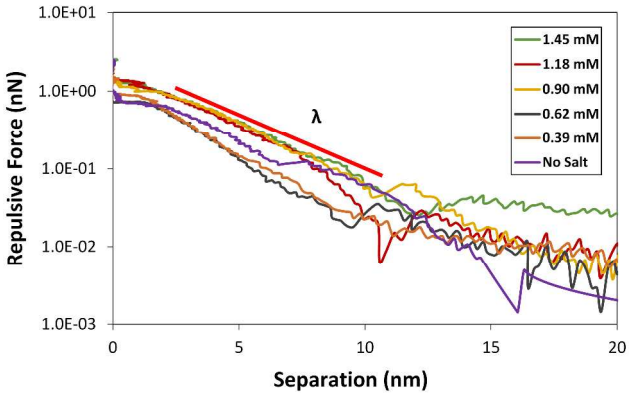

Figure 9. Representative force vs. separation curves for adsorbed 10 mM DAH in the presence of added $MgCl_2$. The red (λ) line shows the regions over which exponential fits were performed.

The repulsive forces displayed in Figure 9 look to be the same as those for our SDS films. If this long range repulsion were the result of electrostatic forces, we would expect a decrease in decay length with added ions rather than an increase.[33] Similarly, the only force that makes sense given our large decay length and surface structure is the steric force. The lack of a split in decay lengths may indicate, similar to what was speculated for SDS, that the micellar brush lengths at the surface are beneath the critical length required for equation (7) to apply. Even though our estimated brush length for DAH is near 24 nm at the highest salt concentration, far higher than those seen in SDS, different surfactants may have different critical brush lengths. For DAH the surface charge density is much lower than it is for SDS, and the counterion density at the surface

is only expected to be around 0.2 M even at the highest salt concentration.[12] When compared with the expected 1.5 M counterion concentration for SDS it becomes clear that the effects of osmotic swelling will be limited for DAH, and behavior will resemble that of an uncharged polymer.

Previous work has shown that the surface density of the adsorbed hemi-micelles increases as surfactant concentration increases.[2-3] This continues until the surfactant concentration in solution nears the CMC, past which the micellar spacing and density no longer change.[3] Images taken of the DAH coated surface show a monotonic decrease in micellar spacing for the adsorbed hemi-micellar structures as $MgCl_2$ is added to solution. This makes some sense, as the concentration of DAH in our trials is always below the CMC[12], whereas it is always above the CMC for our SDS trials. DAH trials above the CMC were not performed, as precipitation readily occurred when salts were added at higher surfactant concentrations. The periodicity of a 10 mM DAH film in the absence of added salt was found to be 7.8 ± 0.2 nm, and was found to decrease to 5.0 ± 0.1 nm when the $MgCl_2$ concentration was 1.34 mM. Since the surface density of these hemi-micelles is closely tied to the value of the CMC, it is appropriate to compare our measured decay lengths to the CMC of DAH as $MgCl_2$ is added (See Figure 10). The data in Figure 10 shows that a 'kink' in our decay length data is replicated in the measured CMC values from our previous work, [12] implying a link between the two quantities through their shared relation to surface density. In the regime of equation (8), the relationship between brush length and surface density can be estimated in a good solvent as[4]

$$L_0 = \Gamma^{\frac{1}{2}} R_F^{\frac{5}{3}} \tag{12}$$

where R_F is the Flory radius. Equation (12) implies that the measured decay length should increase with surface density, which is consistent with our observations for DAH in the presence

of added $MgCl_2$.

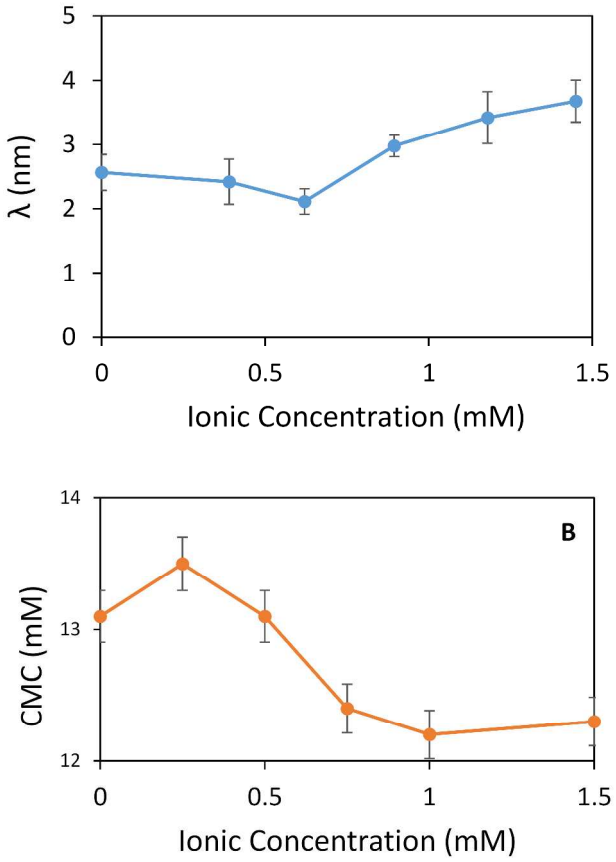

Figure 10. (A) The measured decay length of the force vs. separation curves of adsorbed 10 mM DAH as it changes with $MgCl_2$ concentration and (B) measured values of the CMC of DAH with changing $MgCl_2$ concentration.

Some attempts were also made to estimate the Young's modulus of the DAH film using equations (10) and (11), but we were unable to obtain reliable data about the strain at breakthrough. It appears that the DAH films are much less sturdy than their SDS counterparts at these salt concentrations, and are unable to resist the loading force of the tip for a long enough time to yield usable data. It is plausible that, at higher salt concentrations, more reliable data could be gathered in this region. However, we were unable to continue to concentrations greater

than what is reported for DAH due to the presence of increased turbidity in solution at higher salt concentrations.

Conclusions

We measured the force on an AFM tip as it approached both SDS and DAH hemi-micelles under changing salt concentrations. It was observed, in both cases, that the repulsion experienced by the tip near the surface was exponential when <1 mM of salt was added. Analyzing the decay length of these forces showed that they are likely due to steric forces resulting from collective behavior of these micellar structures, which we refer to as micellar brushes. Their behavior resembles that of a polymer brush, and models intended for such brushes fit very well to our results. The decay lengths were found to change character for SDS at concentrations of salt higher than 1 mM. At these concentrations, the decay lengths increased and behaved similarly to a polyelectrolyte chain. A similar change in behavior was not observed for DAH, as the surface charge and local ionic concentration near the interface is much smaller than for SDS. We also attempted to measure the Young's moduli for these SDS and DAH films. For SDS, we found that the region of contact was too narrow for a detailed mechanical model involving changing Young's moduli at different depths. Instead, we made a one-shot approximation using Sneddon's model while assuming perfectly elastic contact before breakthrough. We found that the Young's modulus of the film was nearly independent of salt concentration. The average over all trials and salt concentrations was found to be 80 MPa, which is consistent with expectations from lipid layers. A histogram of results for these moduli revealed two peaks at 65 MPa and 120 MPa. This may be a result of micellar periodicity along the surface, though this is only speculation. The Young's modulus of DAH could not be obtained from our data, as the film was too fragile to acquire information about deformation before breakthrough.

Overall our results portray a dynamic surface for these micellar films, where we speculate the presence of relatively large (10-20 nm-scale) structures extending into the bulk. This behavior has not previously been reported for SDS films, though they have been the subject of much study. We believe that this will change the overall perspective of repulsive forces from micellar films in future AFM studies. Further work should focus on determining the structure of these micellar brushes and the thermodynamic and kinetic processes that lead to their formation.

Author Information

Corresponding Author

*E-mail: mllongo@ucdavis.edu. Tel: 530-848-9340.

Acknowledgments

Acknowledgment is made to the Donors of the American Chemical Society Petroleum Research Fund for support of this research under grant number 54813-ND5.

References

1. Manne, S.; Cleveland, J. P.; Gaub, H. E.; Stucky, G. D.; Hansma, P. K., Direct Visualization of Surfactant Hemimicelles by Force Microscopy of the Electrical Double Layer. *Langmuir* **1994,** *10* (12), 4409-4413.

2. Wanless, E. J.; Ducker, W. A., Organization of sodium dodecyl sulfate at the graphite−solution interface. *J. Phys. Chem.* **1996,** *100* (8), 3207-3214.

3. Wanless, E. J.; Ducker, W. A., Weak Influence of Divalent Ions on Anionic Surfactant Surface-Aggregation. *Langmuir* **1997,** *13* (6), 1463-1474.

4. Israelachvili, J. N., In *Intermolecular and Surface Forces (Third Edition)*, Academic Press: San Diego, 2011.

5. Israelachvili, J. N.; Wennerstroem, H., Entropic forces between amphiphilic surfaces in liquids. *J. Phys. Chem.* **1992,** *96* (2), 520-531.

6. Fleming, B. D.; Wanless, E. J., Soft-contact Atomic Force Microscopy Imaging of Adsorbed Surfactant and Polymer Layers. *Microsc. Microanal.* **2000,** *6* (2), 104-112.

7. Shulha, H.; Kovalev, A.; Myshkin, N.; Tsukruk, V. V., Some aspects of AFM nanomechanical probing of surface polymer films. *Eur. Polym. J.* **2004,** *40* (5), 949-956.

8. Li, J. K.; Sullan, R. M. A.; Zou, S., Atomic Force Microscopy Force Mapping in the Study of Supported Lipid Bilayers. *Langmuir* **2011,** *27* (4), 1308-1313.

9. Garcia-Manyes, S.; Oncins, G.; Sanz, F., Effect of Ion-Binding and Chemical Phospholipid Structure on the Nanomechanics of Lipid Bilayers Studied by Force Spectroscopy. *Biophys. J.* **2005,** *89* (3), 1812-1826.

10. Das, C.; Sheikh, K. H.; Olmsted, P. D.; Connell, S. D., Nanoscale mechanical probing of supported lipid bilayers with atomic force microscopy. *Phys. Rev. E* **2010,** *82* (4), 041920.

11. Kim, D. H.; Costello, M. J.; Duncan, P. B.; Needham, D., Mechanical properties and microstructure of polycrystalline phospholipid monolayer shells: Novel solid microparticles. *Langmuir* **2003,** *19* (20), 8455-8466.

12. Micklavzina, B. L.; Zhang, S.; He, H.; Longo, M. L., Nanomechanical Characterization of Micellar Surfactant Films via Atomic Force Microscopy at a Graphite Surface. *Langmuir* **2017,** *33* (9), 2122-2132.

13. Hu, K.; Bard, A. J., Characterization of adsorption of sodium dodecyl sulfate on charge-regulated substrates by atomic force microscopy force measurements. *Langmuir* **1997,** *13* (20), 5418-5425.

14. Sasaki, T.; Hattori, M.; Sasaki, J.; Nukina, K., Studies of Aqueous Sodium Dodecyl Sulfate Solutions by Activity Measurements. *Bull. Chem. Soc. Jpn.* **1975,** *48* (5), 1397-1403.

15. Yin, X.; Drelich, J., Surface charge microscopy: novel technique for mapping charge-mosaic surfaces in electrolyte solutions. *Langmuir* **2008,** *24* (15), 8013-8020.

16. Aniansson, G. E., Dynamics and structure of micelles and other amphiphile structures. *J. Phys. Chem.* **1978,** *82* (26), 2805-2808.

17. Biggs, S., Steric and bridging forces between surfaces bearing adsorbed polymer: an atomic force microscopy study. *Langmuir* **1995,** *11* (1), 156-162.

18. Dokukin, M. E.; Kuroki, H.; Minko, S.; Sokolov, I., AFM Study of Polymer Brush Grafted to Deformable Surfaces: Quantitative Properties of the Brush and Substrate Mechanics. *Macromolecules* **2016,** *50* (1), 275-282.

19. Dolan, A. K.; Edwards, S. F., Theory of the Stabilization of Colloids by Adsorbed Polymer. *Proc. R. Soc. London, Ser. A* **1974,** *337* (1611), 509-516.

20. MacKerell Jr, A. D., Molecular dynamics simulation analysis of a sodium dodecyl sulfate micelle in aqueous solution: decreased fluidity of the micelle hydrocarbon interior. *J. Phys. Chem.* **1995,** *99* (7), 1846-1855.

21. Bruce, C. D.; Berkowitz, M. L.; Perera, L.; Forbes, M. D., Molecular dynamics simulation of sodium dodecyl sulfate micelle in water: micellar structural characteristics and counterion distribution. *J. Phys. Chem. B* **2002,** *106* (15), 3788-3793.

22. Balastre, M.; Li, F.; Schorr, P.; Yang, J.; Mays, J. W.; Tirrell, M. V., A Study of Polyelectrolyte Brushes Formed from Adsorption of Amphiphilic Diblock Copolymers Using the Surface Forces Apparatus. *Macromolecules* **2002,** *35* (25), 9480-9486.

23. Tran, Y.; Auroy, P.; Lee, L., Determination of the structure of polyelectrolyte brushes. *Macromolecules* **1999,** *32* (26), 8952-8964.

24. Levchenko, A. A.; Argo, B. P.; Vidu, R.; Talroze, R. V.; Stroeve, P., Kinetics of Sodium Dodecyl Sulfate Adsorption on and Desorption from Self-Assembled Monolayers Measured by Surface Plasmon Resonance. *Langmuir* **2002,** *18* (22), 8464-8471.

25. Goddard, E.; Harva, O.; Jones, T., The effect of univalent cations on the critical micelle concentration of sodium dodecyl sulphate. *Trans. Faraday Soc.* **1953,** *49*, 980-984.

26. de Gennes, P. G., Polymers at an interface; a simplified view. *Adv. Colloid Interface Sci.* **1987,** *27* (3), 189-209.

27. Butt, H.-J.; Kappl, M.; Mueller, H.; Raiteri, R.; Meyer, W.; Rühe, J., Steric forces measured with the atomic force microscope at various temperatures. *Langmuir* **1999,** *15* (7), 2559-2565.

28. Leonenko, Z.; Finot, E.; Ma, H.; Dahms, T.; Cramb, D., Investigation of temperature-induced phase transitions in DOPC and DPPC phospholipid bilayers using temperature-controlled scanning force microscopy. *Biophys. J.* **2004,** *86* (6), 3783-3793.

29. Sokolov, I.; Iyer, S.; Subba-Rao, V.; Gaikwad, R. M.; Woodworth, C. D., Detection of surface brush on biological cells in vitro with atomic force microscopy. *Appl. Phys. Lett.* **2007,** *91* (2), 023902.

30. Szmodis, A. W.; Blanchette, C. D.; Levchenko, A. A.; Navrotsky, A.; Longo, M. L.; Orme, C. A.; Parikh, A. N., Direct visualization of phase transition dynamics in binary supported phospholipid bilayers using imaging ellipsometry. *Soft Matter* **2008,** *4* (6), 1161-1164.

31. Ip, S.; Li, J. K.; Walker, G. C., Phase segregation of untethered zwitterionic model lipid bilayers observed on mercaptoundecanoic-acid-modified gold by AFM imaging and force mapping. *Langmuir* **2010,** *26* (13), 11060-11070.

32. Marsh, D., Elastic curvature constants of lipid monolayers and bilayers. *Chem. Phys. Lipids* **2006,** *144* (2), 146-159.

33. Tulpar, A.; Subramanian, V.; Ducker, W., Decay lengths of double-layer forces in solutions of partly associated ions. *Langmuir* **2001,** *17* (26), 8451-8454.

TOC Graphic

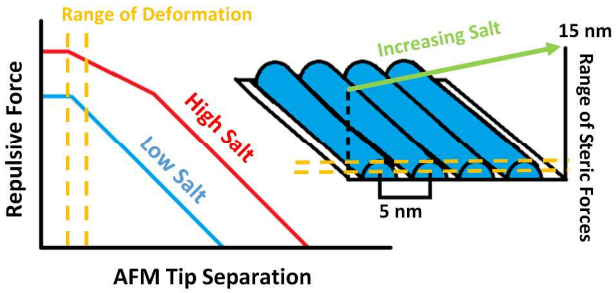
Range of Deformation
Repulsive Force
High Salt
Low Salt
AFM Tip Separation
Increasing Salt
15 nm
5 nm
Range of Steric Forces